Supplementary Information

Modular Nanoparticulate Prodrug Design Enables Efficient Treatment of Solid Tumors Using Bioorthogonal Activation

Miles A. Miller[1,2+*], Hannes Mikula[1,3+], Gaurav Luthria[1,4], Ran Li[1], Stefan Kronister[3], Mark Prytyskach[1], Rainer H. Kohler[1], Timothy Mitchison[5], Ralph Weissleder[1,2,5]

1. Center for Systems Biology, Massachusetts General Hospital, Boston, MA 02114
2. Department of Radiology, Massachusetts General Hospital and Harvard Medical School, Boston, MA 02114
3. Institute of Applied Synthetic Chemistry, Vienna University of Technology (TU Wien), Vienna, Austria.
4. Department of Biomedical Informatics, Harvard Medical School, Boston, MA 02115
5. Department of Systems Biology, Harvard Medical School, Boston, MA 02115

[+]equal contribution

* Correspondence:
Miles A. Miller, PhD
Center for Systems Biology
Massachusetts General Hospital
185 Cambridge St, CPZN 5206
Boston, MA, 02114
617-726-8226
miles.miller@mgh.harvard.edu

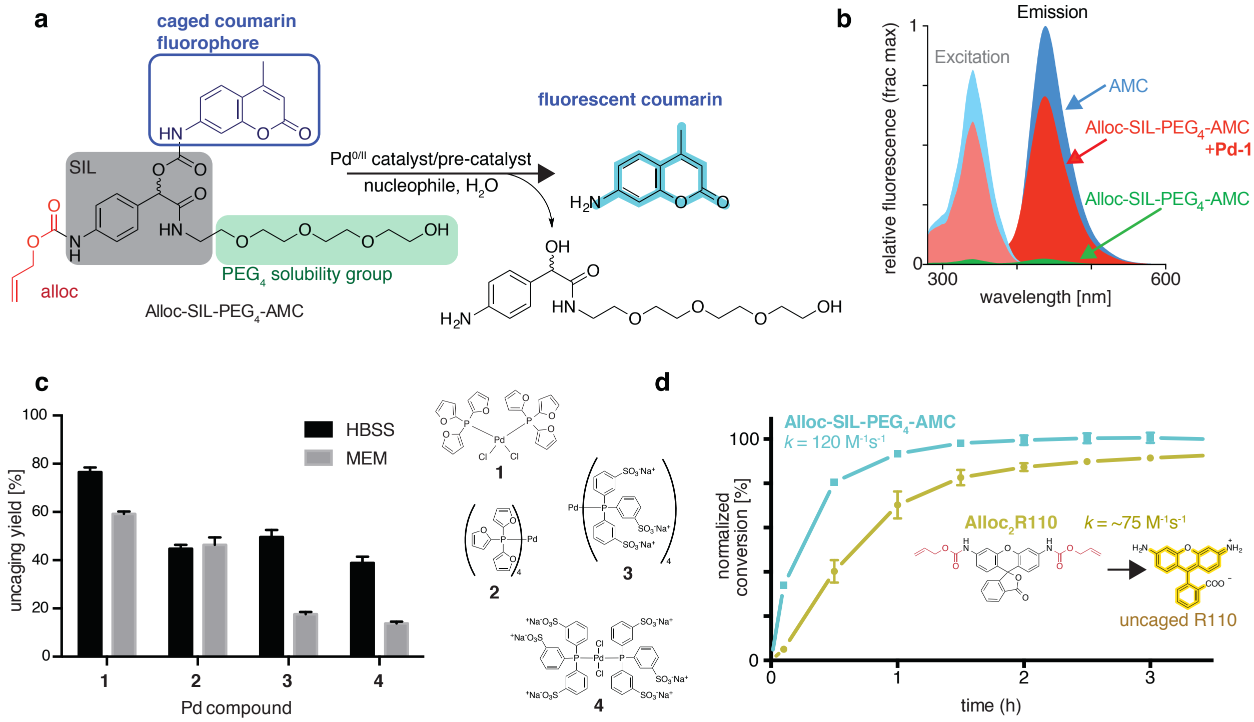

Supplementary Figure S1. A model fluorogenic uncaging reaction reveals the kinetics and efficiency of Pd-mediated deprotection. **a)** Overview schematic of a fluorogenic substrate based on the modular prodrug design. PEG_4 is used to solubilize the substrate in the absence of nano-encapsulation for the *in vitro* screen. In place of the caged drug payload, a caged coumarin is used as a fluorogenic readout of Pd-mediated self-immolation. **b)** Fluorescence excitation and emission spectra show enhanced fluorescence of Alloc-SIL-PEG_4-AMC upon incubation with Pd compound (**Pd-1**, $PdCl_2(TFP)_2$) approaching that of pure, uncaged AMC. **c)** 4 different Pd compounds (10 μM) were tested for their ability to uncage the coumarin substrate (5 μM) in physiologically relevant media (MEM and HBSS) over the course of 10 h. **d)** Using the top performing Pd compound (**Pd-1**, $PdCl_2(TFP)_2$) the kinetics of the coumarin substrate uncaging were compared to the gold-standard reaction of uncaging bis-alloc-protected rhodamine 110 ($Alloc_2R110$).

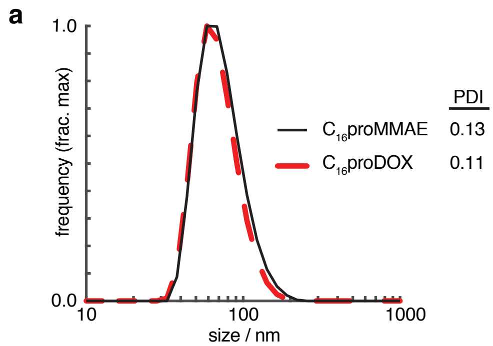

b

	C_{16}proDOX	C_{16}proMMAE
0 h diameter	82.7 ± 1 nm	90.4 ± 3 nm
0 h PDI	0.11	0.13
72 h diameter	66.5 ± 0.2 nm	70 ± 1.3 nm
72 h PDI	0.09	0.11
zeta potential (dI H_2O)	-19 mV	-27 mV
zeta potential (PBS)	-5.3 mV	-4.2 mV
encapsulation efficiency	>90%	>90%
72 h prodrug release	20% ± 6%	9% ± 1%

Supplementary Figure S2. Nanoformulated prodrug size distribution and stability. a) Dynamic light scattering (DLS) describes the distribution in diameter of C_{16}proMMAE and C_{16}proDOX nanoformulations, along with the corresponding polydispersity indices (PDIs); mean of n = 3 replicates shown. **b)** Mean prodrug NP diameter and PDI were measured by DLS before and after 72 h incubation in PBS at 37°C (n=3).

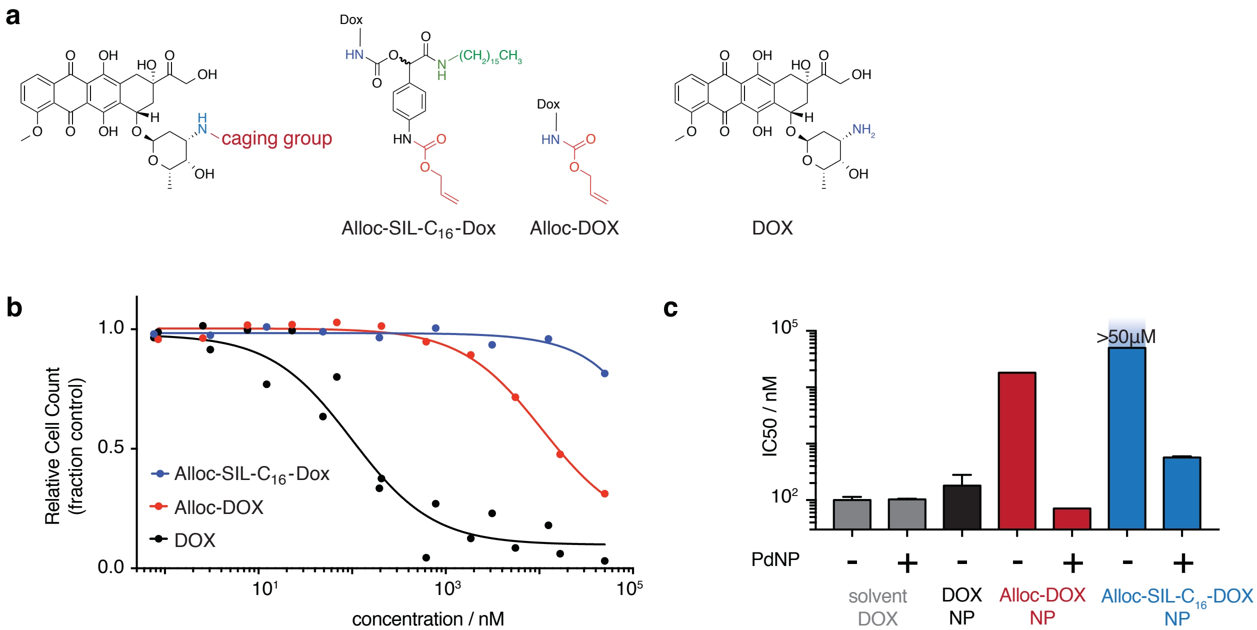

Supplementary Figure S3. Improved prodrug caging increases maximum nontoxic dose in cells. a) Chemical structures of parent doxorubicin and the prodrug caged with Alloc- or Alloc-SIL-C_{16} groups. **b-c)** Viability of HT1080 fibrosarcoma cells was measured following 72 h treatment with doxorubicin and its caged counterparts, shown as a dose-response (b) and quantified (c) according to the concentration yielding 50% reduced viability (IC_{50}), in the presence or absence of 50 μM Pd-NP (n = 2, means ± s.e.m.).

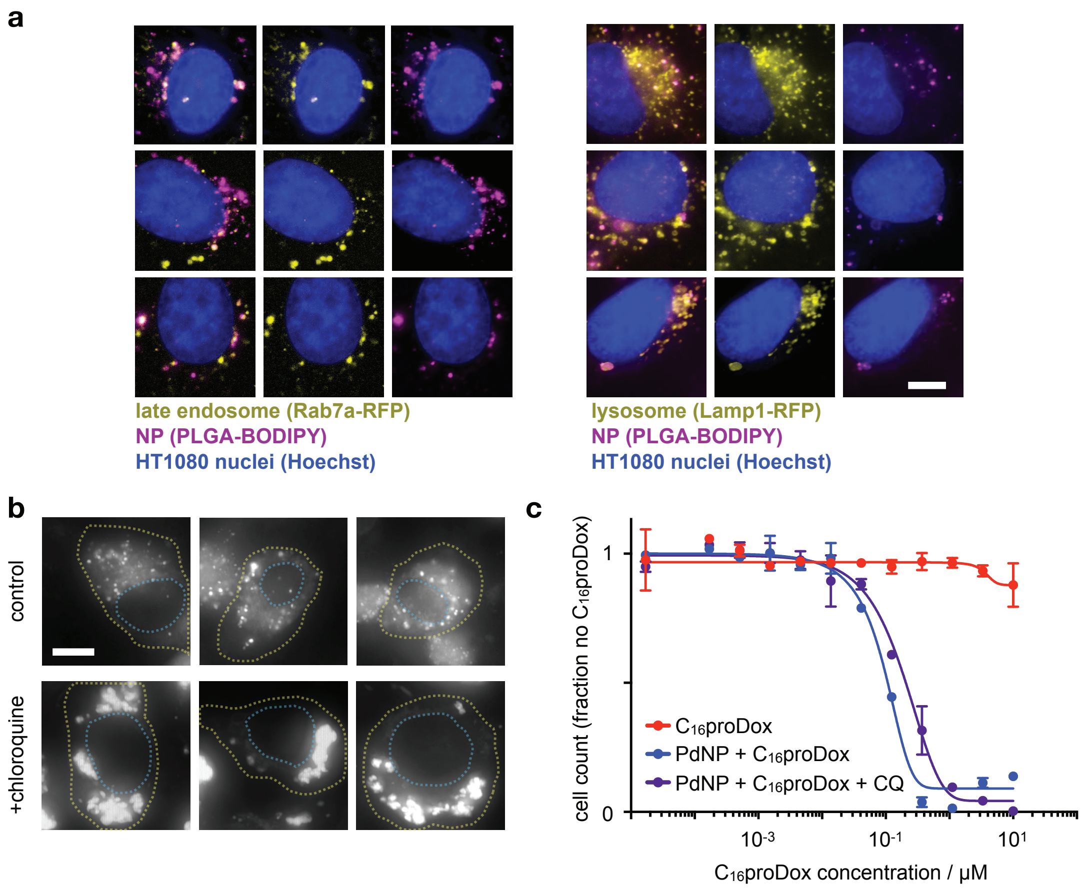

Supplementary Figure S4. Microscopic evaluation of intracellular NP localization. a) Representative live-cell fluorescence microscopy of HT1080 tumor cells expressing either Rab7a-RFP or Lamp1-RFP fusion proteins, after 24 h incubation with a fluorescently labeled NP based on the prodrug formulation (PLGA-PEG+PLGA-BODIPY630). Data correspond with quantitation in Fig. 3a. **b)** Representative images of intrinsic anthracycline fluorescence of C_{16}proDOX after 24 h incubation with HT1080 cells. Yellow and blue outlines denote cell and nuclei boundaries, respectively. Cells were co-treated with 50 µM chloroquine. **c)** Cytotoxicity in HT1080 cells was measured after 72 h incubation with C_{16}proDOX in the presence or absence of 50 µM Pd-NP and 50 µM chloroquine (data are means ± s.e.m.). Both scale bars, 10 µm.

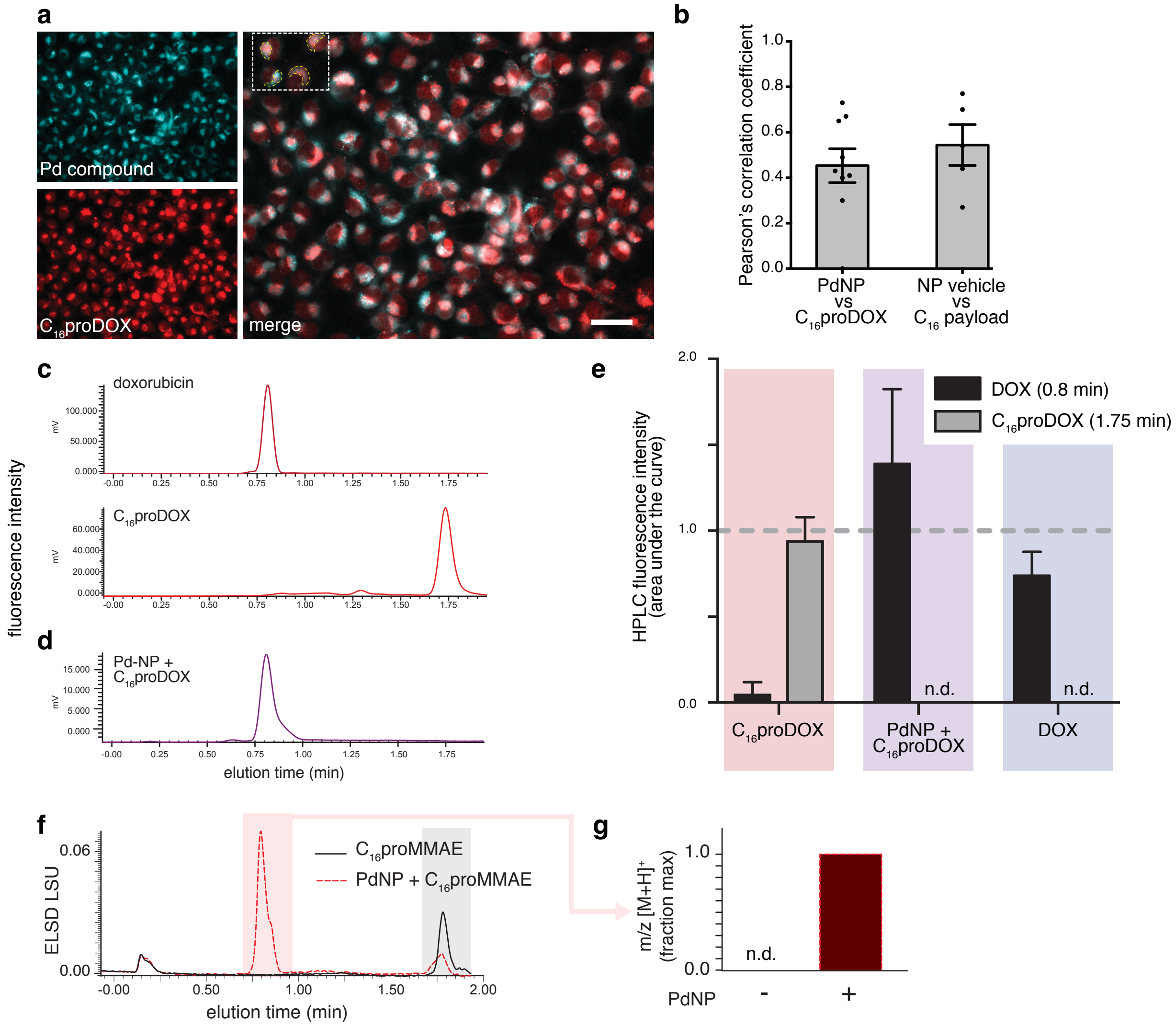

Supplementary Figure S5. Monitoring *in vitro* prodrug activation. a) HT1080 tumor cells were co-treated with C_{16}proDOX and Pd-NP for 24 h, and then imaged by fluorescence microscopy to quantify subcellular drug accumulation based on endogenous fluorescence of anthracycline and Pd compound (scale bar 50 µm). **b)** Pixel-by-pixel co-localization was quantified by selecting ROI over perinuclear regions high in Pd signal based on images as in *a* (see yellow outlined regions in white dashed box for representative ROIs); for comparison, similar co-localization statistics were also computed for comparing PLGA-PEG NP vehicle (labeled with PLGA-BODIPY630) with a fluorescently-labeled, co-encapsulated C_{16} prodrug (C_{16}-Pt(IV)-BODIPY; see [Miller et al., 2015, Nat Commun, 6, 8692]). **c-d)** HPLC fluorescence detection was used to discriminate doxorubicin and C_{16}proDOX based on elution time (c, 50 µM standards), from HT1080 cell lysates following treatment. Representative HPLC fluorimetry trace (d) and corresponding quantification (e; means ± s.d., n = 3) are shown based on peaks at the described elution times. **f)** Representative ELSD detection of C_{16}proMMAE activation by PdNP after 24h. **g)** At red shading in *f*, LC-MS (ESI) calc for MMAE ($C_{39}H_{68}N_5O_7$ {M+H}+ 719.0, found 718.7) only detected with Pd-NP incubation (n=2).

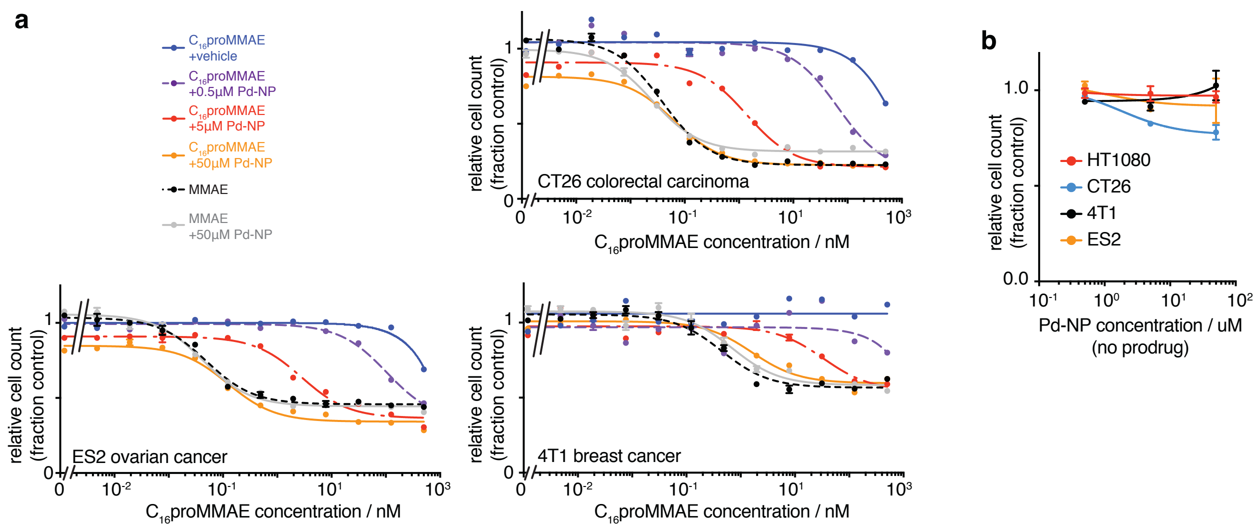

Supplementary Figure S6. Dose-response of PdNP and prodrugs across multiple cancer cell lines. Cytotoxicity was measured using a resazurin-based assay 72 h after treatment. **a)** Viability was measured in response to varying amounts of MMAE or C_{16}proMMAE in the presence or absence of Pd-NP. **b)** Viability was measured across 4 cancer cell lines in response to increasing concentrations of Pd-NP. Data are means ± s.e.m. for all ($n \geq 2$).

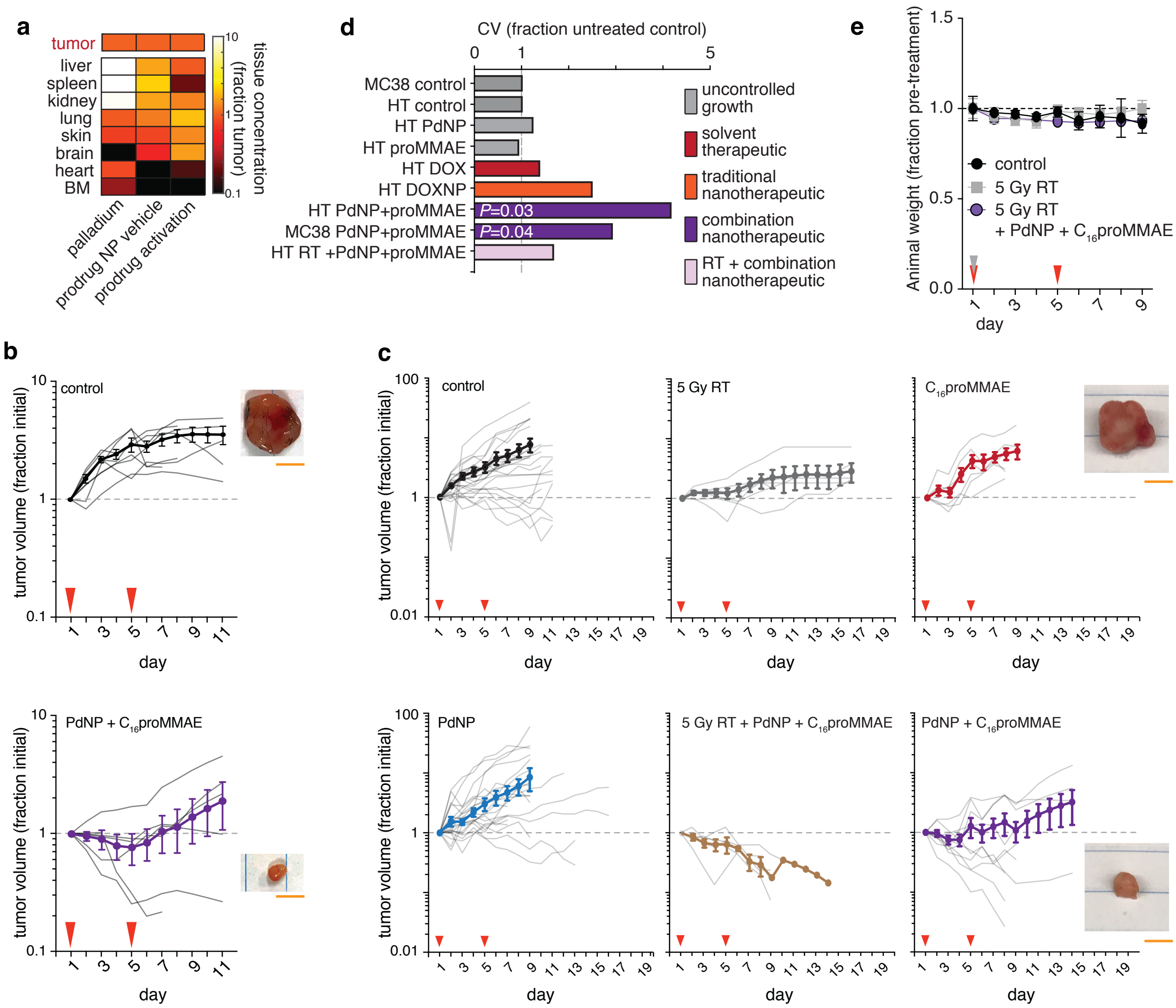

Supplementary Figure S7. Analysis of tumor growth data. a) Tissue concentrations of elemental Pd (left column), the PLGA-PEG vehicle (labeled with PLGA-BODIPY630) of a model nano-encapsulated prodrug substrate (Alloc$_2$R110) (middle column), and the Pd-mediated activation of that substrate (right column) are shown 24 h post-administration in animals bearing HT1080 tumors. Concentration was determined by ICP-MS (for Pd) and reflectance fluorescence microscopy (for prodrug vehicle and prodrug activation), and normalized to the concentration found in tumors (n = 3; see [Miller et al., 2017, Nat Commun, 8, 15906]). Data corresponds to Fig. 6d. **b-c)** Individual tumor growth curves, corresponding to Figs. 5 and 7, are plotted alongside their mean (thick line) and s.e.m. (error bars) for the MC38 (b) and HT1080 (c) models. Red arrows denote the day of treatment. Representative tumor images show unaffected and blocked tumor growth at top and bottom, respectively, corresponding to their adjacent treatment groups (scale bar, 5 mm). **d)** The coefficient of variation (CV) in day 8 tumor volume measurements was calculated across both MC38 and HT1080 tumor models, including using single-treatment controls, solvent based formulation of doxorubicin, and a nanoformulated doxorubicin (see [Miller et al., 2017, Nat Commun, 8, 15906] for DOXNP and DOX treatments and descriptions; n ≥ 5 tumors; F-test to compare variances of the treatment group against their respective no-treatment control). **e)** Weights of animals bearing HT1080 tumors were measured following local low-dose radiation and combination Pd-NP prodrug-NP treatments (n ≥ 3; means ± s.e.m.). Gray and red arrows denote RT and NP treatments.

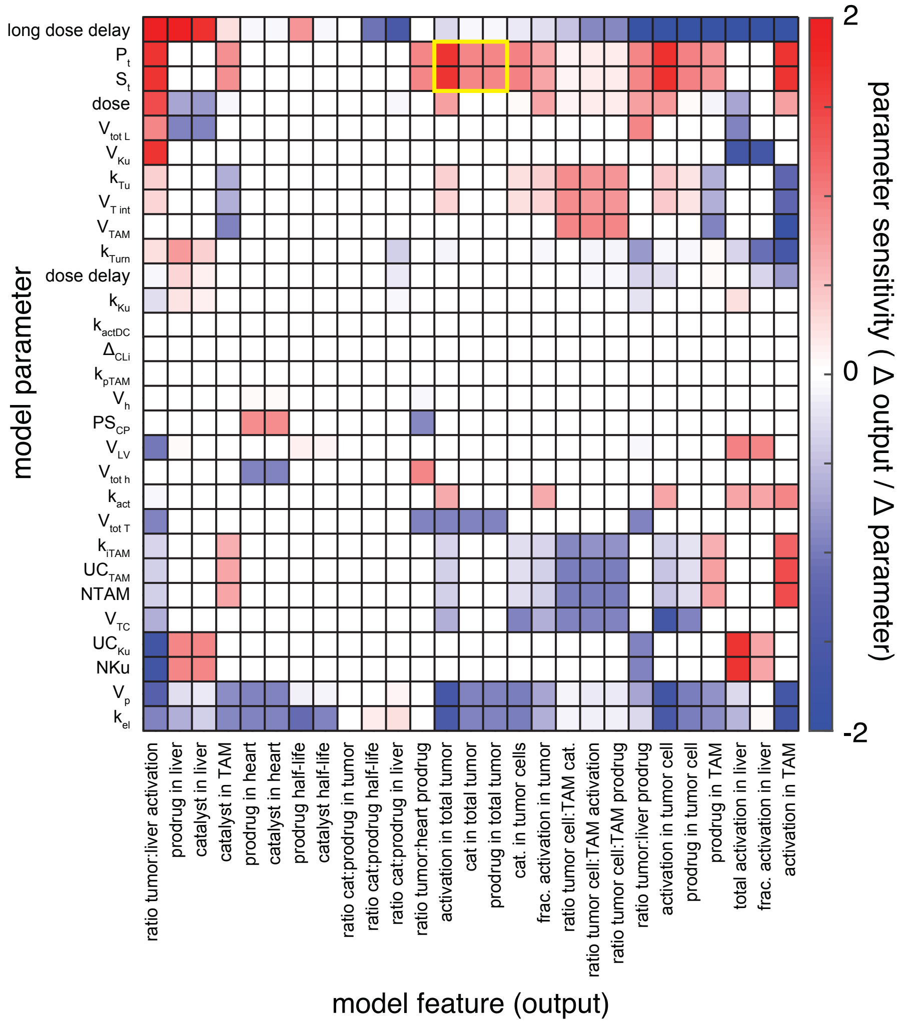

Supplementary Figure S8. Pharmacokinetic model sensitivity analysis. Following parameter optimization, the pharmacokinetic model (see Fig. 6a) was computed while adjusting parameter values by ± 10% (indicated along vertical axis). Change in simulation features 24 h following prodrug administration (horizontal axis) were quantified as a fraction of that feature's value. The ratio of fractional changes in feature values to fractional changes in parameter values (the parametric sensitivities) were then hierarchically clustered and plotted as a heatmap. "Long dose delay" describes changes observed when dose staggering is adjusted from 0 h (co-injection) to 24 h (but without changing the ratio denominator, Δ parameter, for comparison to "dose delay", which examines the impact of adjusting ± 10% around the 5 h dose staggering. The yellow box highlights the relative impacts of P_tS_t on NP accumulation and prodrug activation in the tumor.

parameter	description	optimized value	notes
V_p	vascular volume	0.7 mL	[Baxter et al., 1994, Cancer Res, 54, 1517-28; Hendriks et al., 2012, CPT Pharmacometrics Syst Pharmacol, 1, e15]
k_{el}	plasma elimination	0.01 ± 0.003 min^{-1}	initialized from [Baxter et al., 1994, Cancer Res, 54, 1517-28]
PS_{CP}	plasma / heart interst. transport	$[1.2 \pm 0.4] \times 10^{-6}$ mL min^{-1}	permeability * surface area
V_h	interstitial heart volume	0.019 mL	[Baxter et al., 1994, Cancer Res, 54, 1517-28]
$V_{tot\ h}$	total heart volume	0.133 mL	[Baxter et al., 1994, Cancer Res, 54, 1517-28]
Δ_{CLi}	plasma / liver convective transport	1.1 mL min^{-1}	convective transport [Baxter et al., 1994, Cancer Res, 54, 1517-28]
V_{LV}	volume of liver vasculature	0.095 mL	[Baxter et al., 1994, Cancer Res, 54, 1517-28]
$V_{tot\ L}$	total liver volume	0.95 mL	[Baxter et al., 1994, Cancer Res, 54, 1517-28]
k_{Ku}	2nd-order Kupffer cell uptake	0.016 ± 0.008 $(mg/mL)^{-1}$ min^{-1}	initialized from *in vitro* NP uptake data: [Miller et al., 2017, Sci Transl Med, 9, eaal0225]
P_t	permeability of tumor vasc.	$3.1 \pm 1 \times 10^{-7}$ cm min^{-1}	initialized from [Miller et al., 2015, Sci Transl Med, 7, 314ra183; Miller et al., 2017, Sci Transl Med, 9, eaal0225]
k_{tu}	2nd-order tumor cell uptake	0.018 ± 0.003 $(mg/mL)^{-1}$ min^{-1}	initialized from [Schluep et al., 2009, Proc Natl Acad Sci U S A, 106, 11394-9]
S_t	vasc. surface area of tumor	6 cm^2	[Schluep et al., 2009, Proc Natl Acad Sci U S A, 106, 11394-9]
NKu	# Ku cells	3.5×10^7	[Lopez et al., 2011, Comp Hepatol, 10, 2; Baratta et al., 2009, Histochem Cell Biol, 131, 713-26]
UC_{Ku}	phagocyte uptake capacity	$[2.8 \pm 1] \times 10^{-9}$ mg mL^{-1}	initialized from in vitro saturation experiments [Miller et al., 2017, Sci Transl Med, 9, eaal0225]]
V_{TI}	volume of tumor interstitium	0.105 mL	[Schluep et al., 2009, Proc Natl Acad Sci U S A, 106, 11394-9]
V_{TC}	volume of tumor cells	0.113 mL	[Schluep et al., 2009, Proc Natl Acad Sci U S A, 106, 11394-9; Miller et al., 2015, Sci Transl Med, 7, 314ra183]
$V_{tot\ T}$	total tumor volume	0.3 mL	[Schluep et al., 2009, Proc Natl Acad Sci U S A, 106, 11394-9]
k_{act}	Pd activity in cells	0.008 ± 0.002 $(mg/mL)^{-1}$ min^{-1}	
$k_{act, DC}$	Pd activity in downstream compartment	$[2.4 \pm 5.3] \times 10^{-7}$ $(mg/mL)^{-1}$ min^{-1}	
V_{Ku}	volume of total Ku cells	0.096 ± 0.01 mL	
V_{TAM}	volume of total TAM	0.038 mL	[Schluep et al., 2009, Proc Natl Acad Sci U S A, 106, 11394-9; Miller et al., 2015, Sci Transl Med, 7, 314ra183]
NTAM	# TAM	7.5×10^6	[Miller et al., 2015, Sci Transl Med, 7, 314ra183; Miller et al., 2017, Sci Transl Med, 9, eaal0225]
UC_{TAM}	TAM uptake capacity	$[3.5 \pm 4] \times 10^{-9}$ mg mL^{-1}	initialized from in vitro saturation experiments [Miller et al., 2017, Sci Transl Med, 9, eaal0225]]
k_{iTAM}	2nd-order TAM uptake	0.08 ± 0.05 $(mg/mL)^{-1}$ min^{-1}	
k_{pTAM}	2nd-order TAM uptake	0.016 ± 0.07 $(mg/mL)^{-1}$ min^{-1}	
k_{Turn}	turnover of phagocyte uptake capacity	$[4.5 \pm 1.6] \times 10^{-3}$ min^{-1}	initialized from in vivo saturation: [Miller et al., 2017, Nat Commun, 8, 15906; Sun et al., 2017, Theranostics, 7, 319-328]
k_{qcat} , k_{qpro}	NP i.v. infusion rates	bolus (see methods)	

Supplementary Table S1. Pharmacokinetic computational model parameters. Parameters used in the multi-compartment model are presented alongside references from which the values were taken. For parameters that were optimized to fit the experimental data, values are reported as means ± std. dev. across n = 24 optimization runs.

catalytic NP	y_1 : cat NP in plasma	$dy_1/dt = k_{qcat} / V_p - k_{el}\, y_1 + [\, PS_{CP} (y_2 - y_1) + \Delta_{CLi} (y_3 - y_1) + P_tS_t (y_7 - y_1) - k_{pTAM}\, y_1\, y_9\, V_{TI} \,]\, V_p^{-1}$
	y_2 : cat NP in intst. heart	$dy_2/dt = - PS_{CP} (y_2 - y_1)\, V_h^{-1}$
	y_3 : cat NP in liver vessel	$dy_3/dt = - \Delta_{CLi} (y_3 - y_1)\, V_{LV}^{-1} - k_{Ku}\, y_3\, y_4$
	y_5 : cat NP in Ku cell	$dy_5/dt = k_{Ku}\, y_3\, y_4\, V_{LV} / V_{Ku} - k_{Turn}\, y_5$
	y_6 : cat NP in Ku sink	$dy_6/dt = k_{Turn}\, y_5$
	y_7 : cat NP in tumor intst	$dy_7/dt = P_tS_t (y_1 - y_7)\, V_{TI}^{-1} - k_{Tu}\, y_7 - k_{iTAM}\, y_7\, y_9$
	y_8 : cat NP in tumor cells	$dy_8/dt = k_{Tu}\, y_7\, V_{TI}\, V_{TC}^{-1}$
	y_{10} : cat NP in TAM	$dy_{10}/dt = k_{iTAM}\, y_7\, y_9\, V_{TI}\, V_{TAM}^{-1} - k_{Turn}\, y_{10} + k_{pTAM}\, y_1\, y_9\, V_{TI}\, V_{TAM}^{-1}$
	y_{11} : cat NP in TAM sink	$dy_{11}/dt = k_{Turn}\, y_{10}$
available sites for NP uptake	y_4 : Ku uptake capacity	$dy_4/dt = k_{Turn} (y_5 + y_{5-2} + y_{5-3})\, V_{Ku}\, V_{LV}^{-1} - k_{Ku} (y_{3-2}\, y_4 + y_3\, y_4)$
	y_9 : TAM uptake capacity	$dy_9/dt = k_{Turn} (y_{10} + y_{10-2} + y_{10-3})\, V_{TAM}\, V_{TI}^{-1} - k_{iTAM} (y_7 + y_{7-2})\, y_9 - k_{pTAM} (y_1 + y_{1-2})\, y_9$
prodrug NP	y_{1-2} : prodrug NP in plasma	$dy_{1-2}/dt = k_{q2} / V_p - k_{el}\, y_{1-2} + [\, PS_{CP} (y_{2-2} - y_{1-2}) + \Delta_{CLi} (y_{3-2} - y_{1-2}) + P_tS_t (y_{7-2} - y_{1-2}) - k_{pTAM}\, y_{1-2}\, y_9\, V_{TI} \,]\, V_p^{-1}$
	y_{2-2} : prodrug NP in intst. heart	$dy_{2-2}/dt = - PS_{CP} (y_{2-2} - y_{1-2})\, V_h^{-1}$
	y_{3-2} : prodrug NP in liver vessel	$dy_{3-2}/dt = - \Delta_{CLi} (y_{3-2} - y_{1-2})\, V_{LV}^{-1} - k_{Ku}\, y_{3-2}\, y_4$
	y_{5-2} : prodrug NP in Ku cell	$dy_{5-2}/dt = k_{Ku}\, y_{3-2}\, y_4\, V_{LV} / V_{Ku} - k_{Turn}\, y_{5-2} - k_{act}\, y_5\, y_{5-2}$
	y_{6-2} : prodrug NP in Ku sink	$dy_{6-2}/dt = k_{Turn}\, y_{5-2} - k_{actDC}\, y_6\, y_{6-2}$
	y_{7-2} : prodrug NP in tumor intst	$dy_{7-2}/dt = P_tS_t (y_{1-2} - y_{7-2})\, V_{TI}^{-1} - k_{Tu}\, y_{7-2} - k_{iTAM}\, y_{7-2}\, y_9$
	y_{8-2} : prodrug NP in tumor cells	$dy_{8-2}/dt = k_{Tu}\, y_{7-2}\, V_{TI}\, V_{TC}^{-1} - k_{act}\, y_8\, y_{8-2}$
	y_{10-2} : prodrug NP in TAM	$dy_{10-2}/dt = k_{iTAM}\, y_{7-2}\, y_9\, V_{TI}\, V_{TAM}^{-1} - k_{Turn}\, y_{10-2} - k_{act}\, y_{10}\, y_{10-2} + k_{pTAM}\, y_{1-2}\, y_9\, V_{TI}\, V_{TAM}^{-1}$
	y_{11-2} : prodrug NP in TAM sink	$dy_{11-2}/dt = k_{Turn} y_{10-2} - k_{actDC}\, y_{11}\, y_{11-2}$
depleted prodrug NP	y_{5-3} : depl. prodrug NP in Ku cell	$dy_{5-3}/dt = k_{act}\, y_5\, y_{5-2} - k_{Turn}\, y_{5-3}$
	y_{6-3} : depl. prodrug NP in Ku sink	$dy_{6-3}/dt = k_{actDC}\, y_6\, y_{6-2} + k_{Turn}\, y_{5-3}$
	y_{8-3} : depl. prodrug NP in tu cell	$dy_{8-3}/dt = k_{act}\, y_8\, y_{8-2}$
	y_{10-3} : depl. prodrug NP in TAM	$dy_{10-3}/dt = k_{act}\, y_{10}\, y_{10-2} - k_{Turn}\, y_{10-3}$
	y_{11-3} : depl. prodrug NP in TAM sink	$dy_{11-3}/dt = k_{actDC}\, y_{11}\, y_{11-2} + k_{Turn}\, y_{10-3}$
activated drug	y_{5-4} : act drug in Ku cell	$dy_{5-4}/dt = k_{act}\, y_5\, y_{5-2}$
	y_{6-4} : act drug in Ku sink	$dy_{6-4}/dt = k_{actDC}\, y_6\, y_{6-2}$
	y_{8-4} : act drug in tumor cell	$dy_{8-4}/dt = k_{act}\, y_8\, y_{8-2}$
	y_{10-4} : act drug in TAM	$dy_{10-4}/dt = k_{act}\, y_{10}\, y_{10-2}$
	y_{11-4} : act drug in TAM sink	$dy_{11-4}/dt = k_{actDC}\, y_{11}\, y_{11-2}$

Supplementary Table S2. Pharmacokinetic model equations.

parameter	description	objective value	notes
$t_{1/2,\ cat\ NP}$	circulation half-life, catalytic NP	56 min	time-lapse intravital microscopy of comparable PLGA-PEG NPs in same mouse model [Miller et al., 2017, Sci Transl Med, 9, eaal0225]
$t_{1/2,\ prodrug\ NP}$	circulation half-life, prodrug NP	120 min	time-lapse intravital microscopy of comparable PLGA-PEG NPs in same mouse model, following PdNP[Miller et al., 2017, Nat Commun, 8, 15906]
$t_{1/2}$ ratio	ratio of half-life, cat NP : prodrug NP	0.52 ± 0.05	derived from intravital imaging data in same system (see above); averaged with time-lapse biodistribution data from similar "loading dose" studies [Sun et al., 2017, Theranostics, 7, 319-328; Jang et al., 2016, Biomed Pharmacother, 80, 162-172]
liver uptake	% I.D. / g total liver tissue, catalytic NP	6 ± 3 % ID/g	averaged from a composite of PdNP AAS [Miller et al., 2017, Nat Commun, 8, 15906] and 3 other PLGA-PEG based NPs [Miller et al., 2017, Sci Transl Med, 9, eaal0225; Hrkach et al., 2012, Sci Transl Med, 4, 128ra39]
liver ratio	ratio of liver uptake, cat NP : prodrug NP	1.75 ± 0.3	derived from AAS and fluorescence reflectance imaging of biodistribution in same model [Miller et al., 2017, Nat Commun, 8, 15906]; averaged with biodistribution data from similar "loading dose" studies [Sun et al., 2017, Theranostics, 7, 319-328; Jang et al., 2016, Biomed Pharmacother, 80, 162-172; Liu et al., 2013, Biochim Biophys Acta, 1830, 3447-53; Liu et al., 2015, Sci Rep, 5, 10881]
tumor uptake	% I.D. / g tumor tissue, catalytic NP	0.7 % ID/g	[Miller et al., 2017, Nat Commun, 8, 15906] and consistent with similar PLGA-PEG NPs in the same tumor model [Miller et al., 2017, Sci Transl Med, 9, eaal0225; Miller et al., 2015, Sci Transl Med, 7, 314ra183; Miller et al., 2015, Nat Commun, 6, 8692]
tumor ratio	ratio of tumor uptake, cat NP : prodrug NP	0.56 ± 0.07	averaged with biodistribution data from similar "loading dose" studies [Sun et al., 2017, Theranostics, 7, 319-328; Jang et al., 2016, Biomed Pharmacother, 80, 162-172; Liu et al., 2013, Biochim Biophys Acta, 1830, 3447-53; Liu et al., 2015, Sci Rep, 5, 10881]
fraction tumor activation	ratio of prodrug that activated in the tumor	0.5	[Miller et al., 2017, Nat Commun, 8, 15906]
fraction liver activation	ratio of prodrug activated in the liver	0.25	[Miller et al., 2017, Nat Commun, 8, 15906]
heart uptake	% I.D. / g tumor tissue, catalytic NP	0.11	[Miller et al., 2017, Nat Commun, 8, 15906]
ratio tumor:TAM uptake	ratio of catalytic NP uptake in tumor cells compared to TAM (integrated across all cells)	0.7	intravital microscopy and flow-cytometry using same tumor model and multiple similar PLGA-PEG NPs [Miller et al., 2017, Nat Commun, 8, 15906; Miller et al., 2017, Sci Transl Med, 9, eaal0225; Miller et al., 2015, Sci Transl Med, 7, 314ra183; Miller et al., 2015, Nat Commun, 6, 8692]
ratio of tumor uptake with 5 Gy RT	ratio of catalytic NP accumulating in HT1080 tumors, either with or without 5 Gy irradiation 3 days prior	1.7	intravital microscopy and flow cytometry using same tumor model and multiple similar PLGA-PEG NPs [Miller et al., 2017, Sci Transl Med, 9, eaal0225]

Supplementary Table S3. Pharmacokinetic model optimization parameters. Experimental data from the HT1080 tumor xenograft model, combined with complementary data from similar experimental and NP systems, were used to optimize the computational model (where indicated, data are means ± s.e.m.).

treatment	tumor growth inh.?	tumor shrinkage?	systemic toxicity?	dose (mg/kg)	IC_{50} (nM)	
Pd-NP	-	-	-	50	70,000	*see [Miller et al., 2017, Nat Commun, 8, 15906]
C_{16}proMMAE-NP	-	-	-	1	3,000	
solvent MMAE	n/a	n/a	+	1	0.04	*see [Legigan et al., 2012, Angew Chem Int Ed Engl, 51, 11606-10]
MMAE-NP	n/a	n/a	n/a	n/a	n/a	
RT	+	-	-	5 Gy	*	*see [Miller et al., 2017, Sci Transl Med, 9, eaal0225]
C_{16}proMMAE+Pd	+	-	-	1	0.02	
C_{16}proMMAE+Pd+RT	+	+	-	1		
solvent DOX	+	-	++	10	100	*see [Miller et al., 2017, Nat Commun, 8, 15906]
DOX-NP	+	-	+	10	200	
Alloc-proDOX-NP	-	-	-	10	10,000	
Pd+Alloc-proDOX-NP	+/-	-	-	10	20	
Pd+Alloc-proDOX-NP	+	-	-	30	20	

Supplementary Table S4. Overview of the prodrug strategy efficacy and safety. This table summarizes multiple publications using the HT1080 tumor xenograft model to describe the efficacy and safety profile of the materials described in this and other manuscripts.

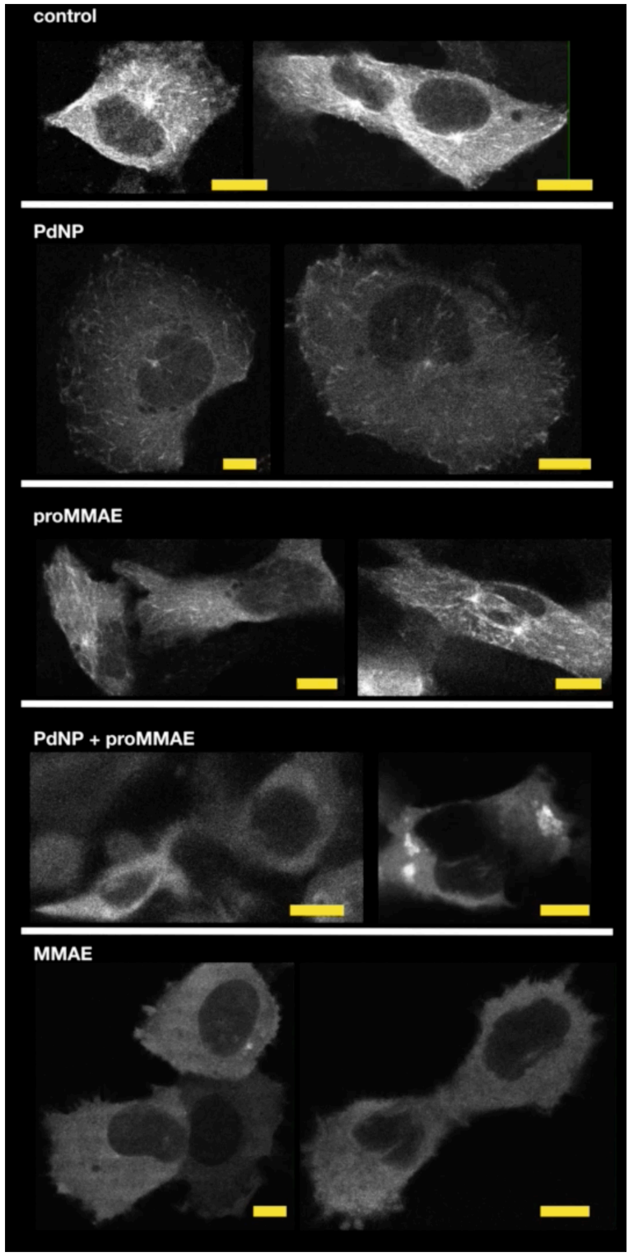

Supplementary Movie S1. Time-lapse microscopy of microtubule comets. Example movies (n=2 shown per condition) are depicted of HT1080 cancer cells expressing EB3-mApple over time. EB3-labeled microtubule comets are visible with control, Pd-NP, and C_{16}proMMAE treatment conditions, but no comets are observed with MMAE or the dual-treatment Pd-NP + C_{16}proMMAE combination. Time and length scales vary slightly across movies, on average showing 1-3 individual cells per movie and 1-5 seconds per movie frame. Scale bar 10 µm. Original resolution reduced for online access.